GEMINI
8-M Telescopes Project

TN-O-G0022

Report on Deformation of the Primary Mirror Cell and Its Effect on Mirror Figure Assuming the Use of an Overconstrained Axial Defining System

Larry Stepp
Optics Group Manager

January 22, 1993

Submitted to the GEMINI 8-meter Telescopes
NSF Independent Review Committee.

ACKNOWLEDGMENTS

I would like to thank Eugene Huang and Myung Cho, who performed the finite-element analysis for this study. Thanks also to Rick McGonegal for providing Figure 1, and to Fred Gillett and Earl Pearson for helpful suggestions and discussions.

INTRODUCTION

The Gemini Optics Group has proposed an overconstrained axial defining system for the primary mirror. This system would be based on a six-zone hydraulic whiffle tree, as illustrated in **Figure 1.** Connecting the mirror to the stiffness of the mirror cell would reduce bending of the mirror caused by wind buffeting. This concept requires any bending of the mirror cell from the effects of changing gravity orientation and thermal gradients to be slow enough to be corrected by the telescope active optics system.

The active optics system will use a wavefront sensor at the Cassegrain focal surface to measure wavefront errors caused by, among other things, bending of the primary mirror. Integration times of approximately 30 seconds would be required to collect enough photons from typical field stars, and to average out atmospheric seeing. Corrections would then be made to the mirror support system, including displacement corrections to each of the six zones of the defining system and force corrections at each of the active force actuators. The overall time required for one cycle of correction in this system is expected to be in the 40-60 second range.

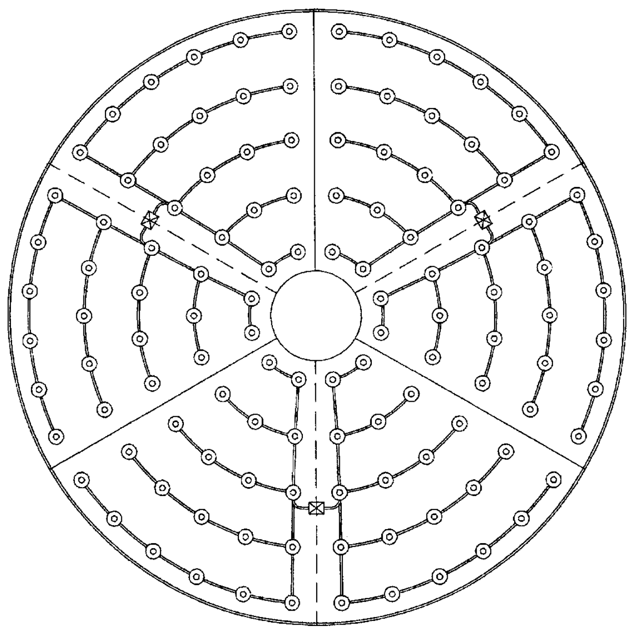

Figure 1. Proposed arrangement of the three-zone / six-zone hydraulic whiffle-tree defining system for the primary mirror.

Questions have been raised about the rate of change of shape of the proposed Gemini mirror cell. If the mirror cell changes shape too rapidly, two adverse effects could occur. First, the accuracy of the wavefront sensing would be affected. Second, the error budget for mirror support errors might be exceeded in less time than one correction cycle.

This report addresses these questions. It describes calculations that have been carried out to predict the nature and rate of change of the mirror cell shape under differing conditions. The effects of these changes on the mirror figure are presented, along with comparisons to the error budget. Thermal distortions are estimated, based on analytical elasticity solutions, and on scaling from previous thermo-elastic studies.

GRAVITY ORIENTATION CHANGES

The mirror cell experiences changes in relative gravity orientation as a result of changes in telescope elevation angle. At issue here is the maximum rate at which this occurs during tracking. Slewing rates are not relevant, because by opening three valves the defining system can be changed into a kinematic three-zone system to allow for the relatively rapid mirror cell flexure that will occur during slewing. **Figure 2** shows the maximum elevation angular velocity during tracking for a telescope on Mauna Kea, which occurs for objects located at +20 degrees declination. To simplify our calculations, we will assume a tracking rate of 0.004 degrees per second for all elevation angles, which is slightly conservative for the worst case at each Zenith angle.

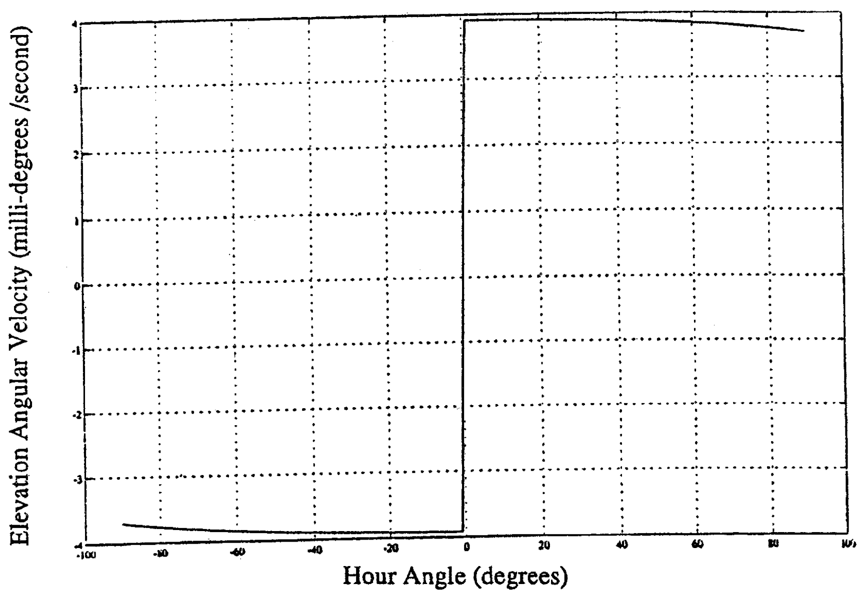

Figure 2. Elevation angular velocity as a function of Zenith angle for tracking through the Zenith, which is the path of maximum elevation angle velocity.

The mirror cell finite-element model used for this study includes the main structural components of the preliminary design. The primary mirror has been included in the model, as has the weight and moment of the Cassegrain instrument assembly.

Gravity-induced flexure of the mirror cell has two orthogonal components, which can be analyzed separately. They are the flexure from gravity at zenith pointing, shown in **Figure 3,** and the flexure from gravity at horizon pointing, shown in **Figure 4.** The horizon-pointing deflection is smaller than the zenith-pointing deflection because the cell is stiffer in the lateral direction, and the level of the support points on the cell has been selected to minimize out-of-plane bending in the horizon-pointing case.

The total deflection (relative to the telescope truss attachment points) at any zenith angle between the zenith and horizon can be determined by the superposition of the zenith-pointing deflection multiplied by the cosine of the zenith angle, plus the horizon-pointing deflection multiplied by the sine of the zenith angle.

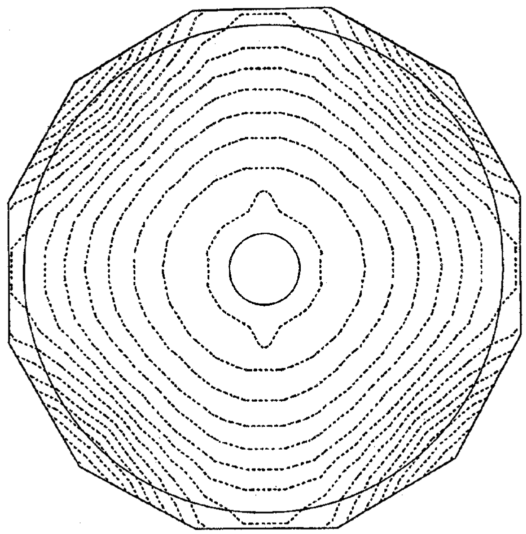

Figure 3. Gravity-induced deflection of the top surface of the primary mirror cell at Zenith-pointing orientation. A circle is drawn in to indicate the relative mirror size.

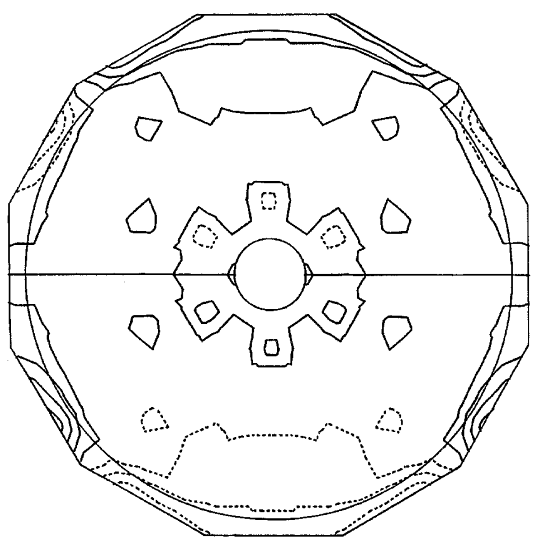

Figure 4. Gravity-induced deflection of the top surface of the primary mirror cell at horizon-pointing orientation. A circle is drawn in to indicate the relative mirror size.

As can be seen by examining Figure 4, the horizon-pointing deflection is anti-symmetric about a center line parallel to the telescope elevation axis, because the structure is symmetric and the applied loads are anti-symmetric. When the average deflections at the support points in each of the six whiffle-tree zones are analyzed, they are also anti-symmetric. The two upper zones have unit positive displacement, the two middle zones have zero displacement and the two lower zones have unit negative displacement. Therefore, the total effect on the mirror is a uniform tilt, which can be neglected because it will automatically be corrected by the secondary mirror tip/tilt system. This means the horizon-pointing deflections do not need to be considered in order to evaluate mirror bending.

To calculate the deformations of the mirror surface, the average displacement of the 20 hydraulic supports in each zone of the whiffle-tree was calculated, then this zonal displacement was transferred to the mirror model. The resulting loading condition applies equal forces on each defining point within a single zone, but different forces from one zone to the next. This analysis was done for the zenith-pointing case, and the resulting mirror surface is shown in **Figure 5.** This represents the amount of deformation that would occur if the mirror figure was optimized at the horizon, the defining system was set as a six-zone whiffle-tree, and the mirror was then tilted to the zenith without any active optics correction. Naturally, if the mirror were then adjusted with the active optics system, this figure deformation would be reduced to levels well within the error budget.

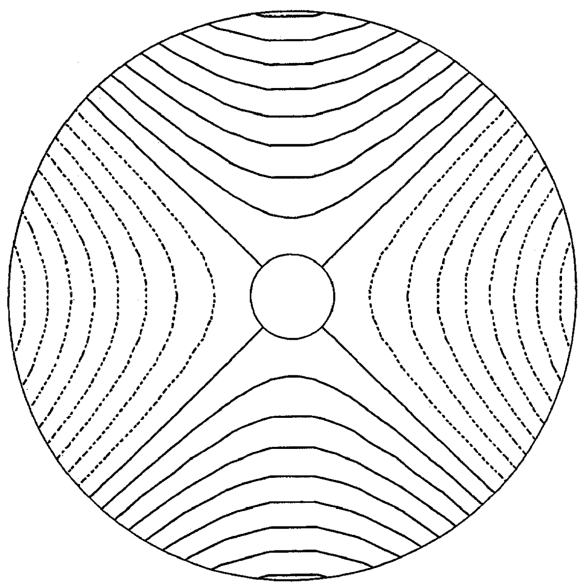

CONTOUR INTERVAL: 1 MICRON
RMS: 3.8 MICRON P-V: 16.8 MICRONS

Figure 5. Deflection of the primary mirror surface that would be caused by the zenith-pointing deformations of the mirror cell shown in Figure 3, if the mirror figure were optimized at the horizon, the defining system overconstraint were engaged, and the mirror were then slewed to the zenith with no active optics correction of figure changes.

Note that the calculated flexure of the mirror under the above conditions is much smaller than the amount of mirror cell flexure that caused it. The eightfold reduction in surface deformation between the cell and the mirror occurs because the defining system is only slightly overconstrained. The system acts as though the mirror and cell are connected at six points equally spaced around a circle. If you imagine the assembly as an active optics system with six actuators, and imagine trying to bend the mirror into different Zernike polynomial terms with just the six actuators, it soon becomes apparent that about the only shapes you could produce would be astigmatism and trefoil. Bending the mirror cell into any other shapes will simply not produce significant bending of the mirror.

To calculate the mirror figure change that would occur in a small time period, the mirror deflection at one zenith angle can be subtracted from the deflection at another, for example, 5.000 and 5.004 degrees zenith angle. **Table 1** presents the results of this type of calculation for one second time intervals at a range of different zenith angles. The encircled energy diameters shown have been determined using

Code V diffraction analysis, but diffraction effects have been subtracted in quadrature in order to be consistent with the error budget.

The maximum figure change per second occurs close to the horizon, but the maximum figure change relative to the error budget occurs at about 35 degrees from the zenith.

Zenith Angle (degrees)	*Mirror Figure Change per second*				*Error Budget*		*Time Before Error Budget is Exceeded (seconds)*	*RMS Surface Error in 30 seconds (nm)*
	Surface		*Encircled Energy Diameter (milli-arcsec)*		*Encircled Energy Diameter (milli-arcsec)*			
	RMS (nm)	*P-V (nm)*	*50%*	*85%*	*50%*	*85%*		
5	0.02	0.1	0.01	0.02	5.06	12.14	466	0.69
10	0.05	0.2	0.02	0.05	5.23	12.55	242	1.38
15	0.07	0.3	0.03	0.07	5.53	13.26	171	2.06
20	0.09	0.4	0.04	0.09	5.95	14.28	140	2.72
25	0.11	0.5	0.05	0.11	6.52	15.65	124	3.36
30	0.13	0.59	0.06	0.13	7.25	17.41	116	3.98
35	0.15	0.67	0.07	0.15	8.18	19.63	114	4.57
40	0.17	0.75	0.08	0.17	9.34	22.4	117	5.12
45	0.19	0.83	0.09	0.18	10.78	25.87	122	5.63
50	0.2	0.9	0.1	0.2	12.59	30.22	132	6.1
55	0.22	0.96	0.1	0.21	14.9	35.75	146	6.52
60	0.23	1.02	0.11	0.23	17.89	42.94	166	6.89
65	0.24	1.06	0.11	0.24	21.91	52.6	194	7.21
70	0.25	1.1	0.12	0.25	27.59	66.21	236	7.48
75	0.26	1.13	0.12	0.25	36.25	87	301	7.69

Table 1. Maximum mirror figure change per second at different zenith angles, with comparisons to the error budgets.

THERMALLY-INDUCED CHANGES

The short response time required for preparation of this report has precluded the chance to run thermo-elastic finite-element models that would be needed to predict mirror cell distortion under a variety of input conditions. However, a lot can be learned from classical elasticity solutions and by scaling from an earlier study of structured mirrors.

For a structure with a flat surface, subjected to a linear temperature gradient defined by the following equation

$$T(x,y,z) = C_1x + C_2y + C_3z$$

the surface deformation is given by[1]:

$$W(r) = -\alpha C_3 r^2/2 + (\alpha C_1 Z_0 r)\cos(\theta) + (\alpha C_2 Z_0 r)\sin(\theta) + \alpha C_3 Z_0^2/2$$

where:

W is the surface deformation
r is the radius position on the surface
θ is the angular position on the surface

α is the coefficient of thermal expansion
Z_0 is the thickness of the structure in the z-direction
C_1, C_2, C_3 are constants

The first term is a curvature change, or defocus. The second and third terms are linear tilts. The fourth term is a piston term that describes the structural thickness change.

As described above, the six-zone mirror defining system cannot transmit any rotationally symmetric figure change to the mirror, so the first term would have no effect. The tilts would be removed by the tip/tilt secondary system. The fourth term, for a mirror cell 1.5 meters thick, made of carbon steel having a CTE of 12 ppm per degree C, would result in a cell thickness growth of 9 microns for a one degree C front to back delta. Since the cell is attached to the telescope structure at about the midpoint between front and back surfaces, the relative piston displacement would be only about 4.5 microns. At a rate of change of temperature delta of one degree C per hour, this would produce a focus shift of 1.25 nm per second. This is small compared to the defocus error budget of 2.4 microns.

Therefore, the effects of uniform temperature gradients in any direction would be negligible.

To find other, higher order types of temperature patterns that <u>would</u> have an adverse effect on the mirror figure, we can refer to a previous study of temperature deformations in structured mirrors[2]. In this study, temperature patterns at three different levels in the model were represented by 9 different Zernike polynomial terms. In all, a total of 61 different combined temperature patterns were imposed on the borosilicate structured mirror. After subtracting out tilt and focus, the average RMS surface deformation per degree of temperature range was 0.50 microns, and the RMS of the amplitude of the 61 RMS surface deformations was 0.72 microns.

The Gemini mirror cell structure is very similar to that of a structured mirror, with front and back faceplates and ribs in between. In structured mirrors, for the same pattern of temperature, front surface deformations scale approximately linearly with the material CTE, and linearly with the aspect ratio of the structure (diameter divided by average thickness)[1]. Therefore, to estimate the bending of the mirror cell we should scale up by a factor of 4 for the ratio of coefficients of thermal expansion, and down by a factor of 1.7 for the smaller aspect ratio of the steel cell, resulting in a total scaling factor of 2.4, if temperature patterns were kept equivalent. In fact, thermal differences are much less likely to build up in the steel cell, because the thermal conductivity of the steel is a factor of 40 higher than borosilicate glass. For equivalent conditions, the steel cell will be much less subject to transient thermal effects than a borosilicate mirror.

Scaling from the referenced study indicates the expected average of a large number of different temperature-induced mirror cell deformations would be 1.2 microns peak-to-valley per degree C. If we assume a rate of temperature pattern change of 1.0 degree C per hour, this would be a change in mirror cell surface of 0.33 nm RMS per second. Much of this deformation would not be transferred to the mirror by the six-zone defining system, for example, any rotationally symmetric shape would have no effect. After examining the plotted deformation shapes in the referenced technical report, I would judge that somewhere between one fourth and one half of this deformation would get through. We will assume the mirror sees half of this deformation, or 0.17 nm RMS per second for a one degree per hour temperature pattern change.

The error budget for this deformation is 0.005 arc seconds for 50% encircled energy, which would correspond to approximately a surface deformation of 11nm RMS. In order to not exceed this error budget in less than 1 14 seconds, to correspond with the worst case gravity-induced error rate, the temperature pattern change should not be greater than 0.57 degree C per hour.

To put these thermal effects in perspective, we should estimate the heat input required to produce this magnitude of temperature pattern change. The mirror cell will contain approximately 35,000 Kg of steel. The specific beat of carbon steel is 450 Joule per Kg per degree C. To heat half the steel in the cell by 0.57 degree C per hour would require the continuous input of 1250 watts if no heat escaped to the rest of the cell or to the environment, and considerably more power under real conditions of heat transfer. In fact, we must already control the heat input and temperature change in the mirror cell to levels smaller than this to avoid local seeing effects, regardless of the type of mirror used.

Fred Gillett calculated that at horizon pointing, one side of the mirror cell could radiate approximately 18 watts per square meter through the slit to the sky. However, because the cell is located inside the center section ring, only a few square meters of the cell could see the sky, resulting in heat transfer of less than 100 watts. Considering the high thermal conductivity of the steel, this amount of heat transfer would not be expected to produce more than about 0.2 degree C per hour of temperature pattern change.

DISCUSSION OF RESULTS

The preliminary error budget for the wavefront sensor anticipates 25 mm RMS error in the measurement and calculation of the surface figure. The worst case gravity-induced figure change in 30 seconds would be 7.7 nm RMS close to the horizon. Close to the Zenith the figure change in 30 seconds would be less than I nm RMS. The figure change in 30 seconds from temperature patterns changing at the rate of 0.57 degrees per hour would be less than 2.9 run RMS. If these two effects are added in quadrature, it is apparent that in 30 seconds there would be only a slight effect on the accuracy of the wavefront sensing at the horizon, where requirements are reduced, and the effects anywhere near the Zenith would be completely negligible.

The relatively small mirror deformations shown in Figure 5 (3.8 micron RMS) indicate that there would be no particular adverse effects of slewing anywhere in the sky without converting the defining system to a three-zone whiffle-tree. Even in going from the zenith to the horizon, stresses in the mirror would be negligible and the mirror figure would still be well within the measurement range of the wavefront sensor. Likewise, there would be no particular adverse effects caused by thermal distortions, even if the whiffle-tree were left in its six-zone configuration for days at a time.

CONCLUSIONS

This analysis indicates that the rate of mirror distortion as a result of bending of the mirror cell transferred to the mirror by the six-zone defining system is well within the current error budget, for worst case tracking rates and for thermal distortions caused by worst case temperature limits imposed by the need to control local seeing effects. Active optics cycle times could be at least twice as long as currently planned, for the worst case conditions, without need for any reallocation of the error budget. No open-loop correction of mirror cell bending effects will be needed, although this technique could be employed if further performance margin is desired.

Changes in mirror surface distortion will not be rapid enough to be a significant limitation on the accuracy of the wavefront sensor.

Care should be taken in the design of systems to be used on the mirror cell, to avoid large nonuniform additions of heat to the structure. Some ventilation of the cell structure, and possible ducting away of heat from specific power sources, should be considered. This will be required as much by the need to control local seeing as by the need to limit mirror cell bending.

This analysis should be repeated after the design of the mirror cell and its associated systems has matured.

REFERENCES

1. E. Pearson and L. Stepp, "Response of large optical mirrors to thermal distributions", SPIE Proceedings, Vol. 748, pp. 215-228, 1987.

2. L. Stepp, "Thermo-elastic analysis of an 8-meter diameter structured borosilicate mirror", NOAO 8-meter Telescopes Engineering Design Study Report No. 1, September, 1989.